J|A|C|S COMMUNICATIONS

Published on Web 07/31/2009

Highly Versatile Rare Earth Tantalate Pyrochlore Nanophosphors

May Nyman,* Mark A. Rodriguez, Lauren E. Shea-Rohwer,* James E. Martin, and Paula P. Provencio

Sandia National Laboratories, P.O. Box 5800, Albuquerque, New Mexico 87185

Received May 11, 2009; E-mail: mdnyman@sandia.gov; leshea@sandia.gov

With the emerging global energy crisis, solid-state lighting has received much attention as a low-energy, robust, long-lifetime, and compact alternative to traditional lighting sources.[1,2] The state-of-the-art solid-state lighting devices would be notably advanced by the discovery of phosphor materials that are optimized for white light-emitting diodes (LEDs). For instance, the blue-excitation LED, in which the yellow-emitting YAG:Ce^{3+} phosphor is excited by an InGaN chip, would improve its poor color-rendering index with the addition of a red phosphor. Red phosphors currently utilized by industry for the GaN LED are nitridosilicates, which have a very broad, deep red emission that does not have a high luminous efficacy of radiation (LER). We have developed a class of pyrochlore-type rare earth tantalate nanoparticles that show great promise as red phosphors for white LEDs. In these materials, the dopant Eu^{3+} can be directly excited by blue light, and we have demonstrated quantum yields (QYs) as high as 78%. The small particle size reduces scattering losses, and the flexibility of the pyrochlore lattice enables tailoring optical properties, such as broadening the blue excitation line width. With this versatile class of oxide-based nanophosphors, we envision being able to meet the challenge of producing efficient blue-pumped solid state lighting (SSL) with high color quality.

The pyrochlore lattice (cubic, $Fd\bar{3}m$) is nominally described as $A_2B_2O_7$, where A is usually a rare earth or alkaline earth metal in an eight-coordinate site, and B is usually a transition metal in a six-coordinate site.[3] It is also described as a double-fluorite structure with an oxygen vacancy. Metals residing in both A-sites and B-sites can take on lower coordination with distortion of the framework: for instance the A-site may become octahedral and the B-site can become tetrahedral.[3] There are also nearly infinite possibilities for site substitutions and vacancies,[4,5] and these versatile materials have been employed as insulators, ion and electron conductors,[6] superconductors,[7] catalysts,[8] robust nuclear waste forms,[9] ion exchangers,[10] etc.

Rare earth tantalates have attractive properties as phosphors, with either stoichiometric[11] or dopant[12−14] concentrations of luminescent metals such as Eu^{3+} or Tb^{3+}. They are chemically and electrochemically stable and can be excited by both blue and UV light. However, they are difficult to produce by methods other than high temperature, solid-state processing. Drawbacks of solid-state synthesis include limitations in discovery of new phases[15] or compositions and difficulty in removing impurities. Furthermore, obtaining nanoparticle or coating forms useful in devices such as LEDs is hampered.

We have developed a hydrothermal tantalate synthesis that produces new structures,[16] forms, and compositions. Aqueous synthetic routes to rare earth tantalates are complicated by the incompatibility of the oxides in solution (tantalate is soluble in base, and rare earth oxides are soluble in acid). Furthermore, even in alkaline solutions the solubility of tantalate is poor and difficult to control. To address these difficulties we utilize the K^+-salt of the $[Ta_6O_{19}]^{8-}$ polyoxometalate ion,[17] which is stable and water-soluble, combined with alkaline-soluble lanthanide citrate complexes. Hydrothermal treatment at 220 °C produces uniform, ∼10−15 nm particles (Figure 1) of $KLnTa_2O_7$:RE with the pyrochlore structure (Ln = Y, Gd, Lu; RE = luminescent rare earth such as Eu^{3+} or Tb^{3+}). We refined the unit cells of the three host-lattice compositions in the $Fd\bar{3}m$ (#227) space group with lattice cell parameters of (a, Å) 10.385(1) ($KLuTa_2O_7$), 10.538(2) ($K_{1-2x}GdTa_2O_{7-x}$; $x = {}^1/_3$), and 10.447(1) ($KYTa_2O_7$). Rietveld refinement of the Lu and Y analogues revealed the K, Lu/Y, and dopant lanthanide are disordered on the eight-coordinate A-site, while Ta resides on the six-coordinate B-site. On the other hand, the eight-coordinate A-site of the Gd analogue is half-occupied with Gd plus the dopant (Eu). The potassium resides in a partially occupied site ∼0.79 Å away from the Gd site and ∼1.5 Å from the partially occupied oxygen site. In essence, the K and Gd are disordered on the A-site, but the potassium is seven-coordinate and off-center toward the vacant oxygen site. This agrees with previous observations: due to electronic effects, Gd-containing pyrochlores have a greater tendency to form defects and disorder than the other lanthanide analogues.[17]

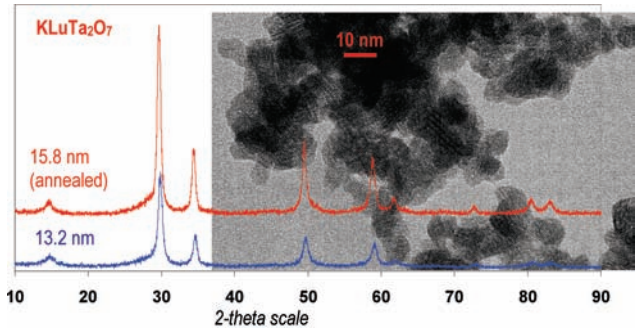

Figure 1. Powder X-ray diffraction pattern of $KLuTa_2O_7$ phosphor nanoparticles from hydrothermal synthesis (bottom) and annealed at 900 °C (top). The nanoparticles only grow slightly upon annealing, as determined by the Scherrer equation. Inset: TEM image of nanoparticles.

The X-ray diffraction pattern of $KLuTa_2O_7$:Eu^{3+} nanoparticles is shown in Figure 1. The Scherrer equation gives a diameter of 13.2 nm, which is consistent with TEM observations. Even after annealing at 900 °C for 2 h, the average diameter is 15.8 nm. FTIR shows the nanoparticles have no surface capping groups, yet the powders are redispersible in DI water. The $KYTa_2O_7$ nanoparticles look similar, but $K_{1-2x}GdTa_2O_{7-x}$ forms larger agglomerates, perhaps due to the magnetism of Gd^{3+} (see Supporting Information (SI)).

Figure 2a shows the photoluminescence excitation and emission (λ_{ex} = 464 nm) spectra of $KLuTa_2O_7$:Eu^{3+}. In the excitation spectrum, the direct, narrowband f−f transitions of Eu^{3+} are more intense than the broad charge transfer band. This is in contrast to the commercial red phosphor YVO_4:Eu^{3+}, where the broad and intense charge transfer band dominates the excitation spectrum. The QY of $K_{1-2x}GdTa_2O_{7-x}$:Eu^{3+} is up to 78% under 464 nm excitation,

10.1021/ja903823w CCC: $40.75

which is nearly 3× greater than that of $YVO_4:Eu^{3+}$ under identical excitation conditions. Notable also is the low thermal quenching of $KLuTa_2O_7:Eu^{3+}$ of only 3% at 130 °C. The emission consists of several narrow band transitions of the Eu^{3+} ion. The most intense of these transitions is at 608 nm, which is nearly ideal for the red component in high luminous efficacy white LEDs, and there is little unwanted emission in the deep-red range. Because of this reduced deep-red emission, the LER is superior to that of $YVO_4:Eu^{3+}$ (300 lm/W_{em} for $KLuTa_2O_7:Eu^{3+}$ and 217 lm/W_{em} for $YVO_4:Eu^{3+}$).

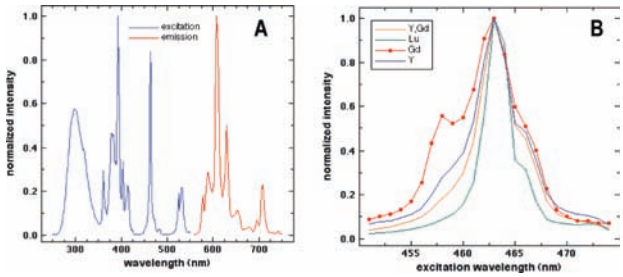

Figure 2. (A) Photoluminescence excitation (blue) and emission (red) of $KLuTa_2O_7:Eu^{3+}$ (spectra for Gd and Y analogues are similar) **2b**. (B) Comparison of line widths of blue-excitation peaks for (Gd,Y), Y, Gd, and Lu analogues.

The blue excitation bandwidth is important for SSL lighting applications. If it is too narrow, it will be difficult to absorb sufficient InGaN LED emission energy. Figure 2b shows the blue excitation peak for the different rare earth pyrochlore analogues. The Gd analogue excitation line width is nearly 2× that of the Lu analogue. This increased width reduces the need for emission wavelength control of the LEDs and increases the absorption cross section of the phosphor.

The QYs for Eu-doped Lu, Y, and Gd analogues under blue excitation are plotted in Figure 3 as a function of Eu concentration (determined by energy dispersive spectroscopy; see SI). While the Y and Lu analogues peak at ~65% QY (for 10% Eu-doping of the K/Ln site), the Gd analogue quenches at a much higher Eu concentration. We attribute this difference to the structure of the Gd analogue: Eu^{3+}-site distortion gives rise to enhanced photoluminescence.[18] Regardless, all these pyrochlore analogues have excellent QY values (approaching 80%), especially for nanoparticle forms that can suffer QY loss from poor crystallinity or surface effects.

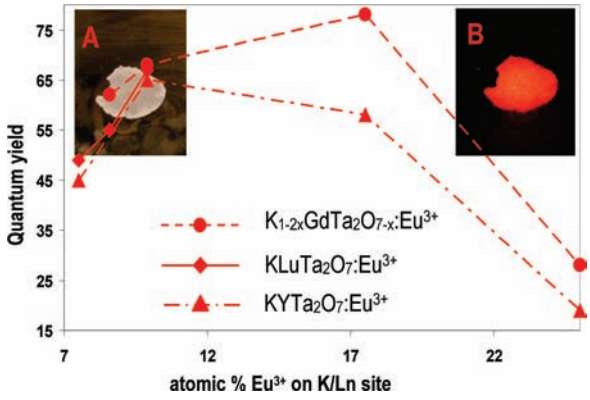

Figure 3. Quantum yield of Y, Gd, and Lu analogues as a function of Eu-doping. Lu analogue in room light (A) and backlit by a UV lamp (B).

Because the relevant 4f−4f transitions in Eu^{3+} are formally electric dipole forbidden, its direct absorption cross section is small,[18] estimated to be on the order of $\sigma \approx 3.8 \times 10^{-20}$ cm^{-2}, and the PL lifetimes are generally ~1 ms. In fact, we measured lifetimes of 1.6, 1.8, and 2 ms for Ln = Lu, Gd, and Y/Gd, respectively, under blue LED excitation. These long lifetimes could cause the emission to saturate when excited with the high light intensities of commercial LEDs, ~200W/cm^2, but our calculations show that saturation is a concern only at much higher intensities, due to the low absorption cross section of Eu^{3+}.

Finally, we note that semitransparent nanoparticle monoliths (in Figure 3A and B) of the Lu analogue can be prepared, which introduces new possibilities for engineering these materials into useful forms, such as scintillators. We achieve semitransparency by doubling the amount of the lutetium salt in the precursor mixture, which forms core−shell, $KLuTa_2O_7:Eu^{3+}-Lu_2O_3$ nanoparticles (see SI). Lu_2O_3, which is also cubic ($I\bar{3}a$) with a similar unit cell dimension (a = 10.358 Å) as $KLuTa_2O_7$, is a transparent oxide.[19] We know the Eu^{3+} resides in the $KLuTa_2O_7$ core because the adsorption and emission spectra of $Lu_2O_3:Eu^{3+}$ are completely different than those of the pyrochlores. For instance, the excitation spectrum of $Lu_2O_3:Eu^{3+}$ features a large O →Eu charge-transfer band and little blue absorption.[19] $(Y,Gd)_2O_3$ and Gd_2O_3 are also transparent,[20] so these nanophosphor assemblies are also being further developed.

We have shown that rare earth tantalate pyrochlore nanoparticles $KLnTa_2O_7:Eu^{3+}$ are new promising red-emitting phosphors for blue-excitation white LEDs. Further, the flexibility of the pyrochlore lattice enables tailoring of the photoluminescence to accommodate specific device requirements. Photocatalysis[21] and ionic conductivity[6] are other applications that are potentially fruitful and currently under investigation for this new class of nanoparticle materials.

Acknowledgment. Sandia is a multiprogram laboratory operated by Sandia Corporation, a Lockheed-Martin Company, for the United States DOE under Contract No. DE-AC04-94AL85000. Partial funding obtained from DOE NETL (DE-PS26-06NT42942).

Supporting Information Available: Document containing experimental details and complete ref 1. Crystallographic information files (cif) for $K_{1-2x}GdTa_2O_{7-x}$, $KYTa_2O_7$, and $KLuTa_2O_7$. This material is available free of charge via the Internet at http://pubs.acs.org.

References

(1) Phillips, J. M.; et al. *Laser Photonics Rev.* **2007**, *1*, 307–333.
(2) Schubert, E. F.; Kim, J. K. *Science* **2005**, *308*, 1274–1278.
(3) Subramanian, M. A.; Aravamudan, G.; Subba-Rao, G. V. *Prog. Solid State Chem.* **1983**, *15*, 55–143.
(4) Maillard, P.; Tessier, F.; Orhan, E.; Chevire, F.; Marchand, R. *Chem. Mater.* **2005**, *17*, 152–156.
(5) Roth, R. S.; Vanderah, T. A.; Bordet, P.; Grey, I. E.; Mumme, W. G.; Cai, L.; Nino, J. C. *J. Solid State Chem.* **2008**, *181*, 406–414.
(6) Deng, Z. Q.; Niu, H. J.; Kuang, X. J.; Allix, M.; Claridge, J. B.; Rosseinsky, M. J. *Chem. Mater.* **2008**, *20*, 6911–6916.
(7) Hanawa, M.; Muraoka, Y.; Tayama, T.; Sakakibara, T.; Yamaura, J.; Hiroi, Z. *Phys. Rev. Lett.* **2001**, 87.
(8) Ikeda, S.; Itani, T.; Nango, K.; Matsumura, M. *Cat. Lett.* **2004**, *98*, 229–233.
(9) Ewing, R. C. *Can. Mineral.* **2001**, *39*, 697–715.
(10) Moller, T.; Clearfield, A.; Harjula, R. *Chem. Mater.* **2001**, *13*, 4767–4772.
(11) Roof, I. P.; Smith, M. D.; Park, S.; zur Loye, H. C. *J. Am. Chem. Soc.* **2009**, *131*, 4202–4203.
(12) Thomas, M.; Prabhakar-Rao, P.; Deepa, M.; Chandran, M. R.; Koshy, P. *J. Solid State Chem.* **2009**, *182*, 203–207.
(13) Yan, B.; Xiao, X. *J. Alloys Compd.* **2007**, *433*, 251–255.
(14) Xiao, X.; Yan, B. *J. Mater. Res.* **2008**, *23*, 679–687.
(15) One exception to the inability to produce new phases is recent molten-salt syntheses of new rare earth tantalates (i.e., see ref 11).
(16) Nyman, M.; Rodriguez, M. A.; Alam, T. M.; Anderson, T. M.; Ambrosini, A. *Chem. Mater.* **2009**, *21*, 2201–2208.
(17) Jiang, C.; Stanek, C. R.; Sickafus, K. E.; Uberuaga, B. P. *Phys. Rev. B* **2009**, *70*, 104203.
(18) Lee, G. H.; Kang, S. H. *J. Electrochem. Soc.* **2006**, *153*, H105–H109.
(19) Chen, Q.; Shi, Y.; An, L.; Chen, J.; Shi, J. *J. Am. Ceram. Soc.* **2006**, *89*, 2038–2042.
(20) Greskovich, C.; Duclos, S. *Annu. Rev. Mater. Sci.* **1997**, *27*, 69–88.
(21) Osterloh, F. E. *Chem. Mater.* **2008**, *20*, 35–54.

JA903823W